Nuclear Physics B144 (1978) 269–286

Δ(1232) PRODUCTION BY VIRTUAL PHOTONS

K. WACKER *, G. DREWS, J. KNOBLOCH **, H. NAGEL ***, E. RABE, W.-D. SCHLATTER ** and H. SPITZER
II. Institut für Experimentalphysik der Universität Hamburg

C.K. CHEN ‡, J. KNOWLES, D. MARTIN, J.M. SCARR and I.O. SKILLICORN
University of Glasgow, Glasgow

P. JOOS, A. LADAGE, H. MEYER * and G. WOLF
Deutsches Elektronen-Synchrotron DESY, Hamburg

Received 17 July 1978

The reaction $\gamma_v p \to p\pi^+\pi^-$ was studied in the W, Q^2 region 1.3 to 2.8 GeV, 0.3 to 1.4 GeV^2 using the streamer chamber at DESY. An analysis of $\Delta^{++}(1232)$ and $\Delta^0(1232)$ production *via* $\gamma_v p \to \Delta\pi$ is presented. The W dependence, production angular distribution and decay distribution of Δ^{++} in the channel $\Delta^{++}\pi^-$ is similar to that found in photoproduction. At small momentum transfers the Q^2 dependence of Δ^{++} production follows that of the ρ propagator as predicted by VDM; at large momentum transfer there is little Q^2 dependence. The W dependence of Δ^0 production and its ratio with respect to Δ^{++} production is similar to that found in photoproduction.

1. Introduction

In this paper we present final results on Δ(1232) production by virtual photons *via* the channels

$$\gamma_v p \to \pi^- \Delta^{++} , \tag{1}$$

$$\gamma_v p \to \pi^+ \Delta^0 . \tag{2}$$

The experiment, which used the DESY streamer chamber to study inelastic electron-proton scattering, covered hadron c.m.s. energies, W, between threshold and

* Now at Bergische Universität, Wuppertal, Germany.
** Now at CERN, Geneva, Switzerland.
*** Now at Beiersdorf AG, Hamburg, Germany.
‡ Now at Argonne National Laboratory, Argonne, Ill., USA.

2.8 GeV, and values of the photon mass squared, $-Q^2$, from -0.3 to -1.4 GeV^2. Final results on ρ and ω production, and on inclusive $\pi^{\pm}$ production have already been published [1–3]. We have also reported studies of reaction (1) near threshold in which we have determined the Q^2 dependence of the $\gamma_v p \to \Delta^{++}\pi^-$ contact interaction and the Q^2 dependence of the nucleon axial-vector form-factor [4,5].

Here we present our experimental results on channels (1) and (2) and compare them with photoproduction. Photoproduction of $\Delta^{++}\pi^-$ states below $W \simeq 1.8$ GeV is known to be dominated by a $\gamma p \Delta \pi$ contact interaction and by s-channel resonance formation [6]. At higher energies the photoproduction process has the characteristics of one-pion exchange; that is one finds an E_γ^{-2} dependence of the production cross section [7] and dominance of unnatural parity exchange in the t-channel [8]. In the framework of vector dominance (VDM) it is assumed that the above processes are mediated by incident virtual rho mesons. If VDM holds both for photo- and electroproduction, we expect the cross section to vary like the rho propagator, $(m_\rho^2 + Q^2)^{-2}$, as Q^2 changes. However, to the extent that longitudinal photons can be neglected, other characteristics of Δ^{++} electroproduction, such as the production angular distribution and the decay distribution, would be the same as in photoproduction. In this paper, we study the Q^2 dependence of the Δ cross section, and its angular distribution, with the object of testing whether this vector-dominance approach is in agreement with our data.

The paper is organized as follows: first we review the experimental procedure (sect. 2). In sect. 3 we discuss resonance production in the reaction $\gamma_v p \to p\pi^+\pi^-$. In sect. 4 we give the Δ^{++} production cross section as a function of W, Q^2 and t, and we discuss the Δ^{++} decay distribution. The characteristics of Δ^0 production are given in sect. 5 and a summary of Δ production in sect. 6.

2. Experimental procedure

A detailed description of the setup and the event analysis has been given in refs. [9,10]. A 7.2 GeV electron beam traversed a 9 cm long liquid hydrogen target inside a streamer chamber. The streamer chamber, of 1 m length, was in a magnetic field of 1.8 T. Two arrays of trigger counters, lucite Čerenkov counters and lead scintillator sandwich shower counters detected the scattered electron. About 70% of the data were taken with a proportional wire chamber added to each of the two detector arms [11]. With the proportional chambers the average measurement error of the scattered electron's momentum was $\Delta p = \pm p^2/p_{\mathrm{MDM}}$ with $p_{\mathrm{MDM}} \simeq 250$ GeV/c; the error on the scattering angle was about ±1 mrad.

Approximately 360 000 pictures were taken with a total flux of $3.3 \cdot 10^{12}$ electrons incident on the target. The event analysis was similar to that used in bubble-chamber experiments. A total of ~9100 elastic and ~46 700 inelastic ep scattering events were obtained *.

* 2-prong events were analyzed on 50% of the film only.

Δ production *via* reactions (1) and (2) was studied in the final state

$$ep \to ep\pi^+\pi^- . \tag{3}$$

The events selected for reaction (3) were required to give a 4C fit ($\chi^2 < 38$) consistent with the observed track ionization. For 10% of the events of reaction (3) one track was obscured by the target box or by flares. To be accepted as reaction (3) these events had to give a 1C fit ($\chi^2 < 28$). A total of 7383 events, which satisfied these selection criteria, were found in the kinematical region $1.3 < W < 2.8$ GeV, $0.3 < Q^2 < 1.4$ GeV^2.

Two independent Monte Carlo programs were used to determine the loss of events due to radiation and the selection procedure. The Monte Carlo events were processed through the geometric and kinematic reconstruction programs in the same way as the measured events. The contamination of events from other reactions giving an acceptable fit for reaction (3) was found to be smaller than 5%. The radiative corrections were estimated in the peaking approximation. The corrections amount typically to a +23% contribution from external and internal Bremsstrahlung and a −7% contribution from vertex and propagator corrections [12] (see ref. [10] for details).

Cross sections were determined by normalizing the total number of inelastic ep events (after correcting for acceptance and radiative effects) to the total inelastic ep cross section measured in a single-arm experiment [13]. The errors given below are statistical only. A systematic uncertainty of ±10% has to be added which covers the uncertainties from event selection (5%), radiative corrections (4%) and cross-section normalization (7%).

3. General characteristics of the reaction $\gamma_V p \to p\pi^+\pi^-$

3.1. Definition of the cross section

In the notation of Hand [14] the differential cross section $d^2\sigma(f)/dQ^2\, dW$ for electroproduction of a final state f is expressed in terms of the cross sections $\sigma_T(f)$ and $\sigma_L(f)$ for production of f from scattering of transverse and longitudinal virtual photons on protons by

$$\frac{d\sigma(f)}{dQ^2 dW} = \frac{\pi}{EE'} \frac{W}{m_p} \Gamma_T \{\sigma_T(Q^2, W, f) + \epsilon\sigma_L(Q^2, W, f)\} , \tag{4}$$

where E, E' are the lab energies of the incident and scattered electron, m_p is the mass of the proton, Γ_T measures the flux of transverse photons,

$$\Gamma_T = \frac{\alpha}{4\pi^2} \frac{E'}{E} \frac{W^2 - m_p^2}{m_p Q^2} \frac{1}{1-\epsilon}, \tag{5}$$

with

$$\epsilon = \left[1 + 2\frac{\nu^2 + Q^2}{4EE' - Q^2}\right]^{-1}, \qquad Q^2 >> m_e^2, \tag{6}$$

$$\nu = E - E'.$$

For the majority of the events the polarization parameter, ϵ, lies in the range 0.85 – 0.95. The value of ϵ is fixed for a given Q^2 and W, therefore no model independent separation of σ_T and σ_L can be made in this experiment. The $\gamma_v p$ cross section is defined as

$$\sigma(Q^2, W) = \sigma_T(Q^2, W) + \epsilon\sigma_L(Q^2, W). \tag{7}$$

3.2. Resonance production in the reaction $\gamma_v p \to p\pi^+\pi^-$

The channel cross sections and mass distributions for various Q^2, W intervals for the channel $\gamma_v p \to p\pi^+\pi^-$ have been given elsewhere [1]. The mass distributions indicate strong $\Delta^{++}(1232)$ and ρ^0 production plus a small amount of Δ^0 production. The cross sections for Δ^{++}, Δ^0 and ρ^0 production were determined by a maximum-likelihood fit to the Dalitz-plot density:

$$\mathrm{d}N(M^2_{p\pi^+}, M^2_{\pi^+\pi^-}) = [a_{\Delta^{++}}F_{\Delta^{++}}(M_{p\pi^+})\, W_\Delta(\cos\theta_{H\Delta}) + a_{\Delta^0}F_{\Delta^0}(M_{p\pi^-})$$
$$+ a_\rho F_\rho(M_{\pi^+\pi^-})\, W_\rho(\cos\theta_{H\rho}) + a_{ps}F_{ps}] \times \mathrm{d}M^2_{p\pi^+}\, \mathrm{d}M^2_{\pi^+\pi^-}. \tag{8}$$

The fitted parameters, a, measure the size of the Δ^{++}, Δ^0, ρ and phase-space contributions; F_Δ, F_ρ describe normalized Breit-Wigner distributions, e.g., for the Δ

$$F_\Delta = B_\Delta / I_\Delta,$$

with

$$B_\Delta(m) = \frac{m}{q}\frac{\Gamma(m)}{(m_\Delta^2 - m^2)^2 + m_\Delta^2\Gamma^2(m)}.$$

Here m is the πp effective mass and $\Gamma(m) = \Gamma_\Delta(q/q_0)(m_\Delta/m)\, U_1(qr)/U_1(q_0 r)$; q and q_0 are the π momenta in the πp rest frame at the mass m and m_Δ, respectively, and

$$U_1(x) = \tfrac{1}{2}x^2\left(\frac{2x^2 + 1}{4x^2}\ln(4x^2 + 1) - 1\right)$$

with $r = 2.2\ \mathrm{GeV}^{-1}$ [15].

The normalization constant I_Δ is obtained for a given event from an integration over the Dalitz plot

$$I_\Delta = \int B_\Delta W_\Delta \mathrm{d}M^2_{p\pi^+}\mathrm{d}M^2_{\pi^+\pi^-}.$$

$W_\Delta(\cos\theta_{H\Delta})$ describes the Δ^{++} decay angular distribution in the helicity frame and is given by

$$W_\Delta(\cos\theta_{H\Delta}) = (\tfrac{1}{4} + r_{33}^{04}) + (\tfrac{3}{4} - 3\,r_{33}^{04})\cos^2\theta_{H\Delta}\ ,$$

where $\theta_{H\Delta}$ is the polar decay angle of the Δ with respect to the line of flight of the Δ and the density matrix element r_{33}^{04} lies between 0 and 0.5. $W_\rho(\cos\theta_{H\rho})$ is the corresponding distribution for the ρ decay [1].

The quantity F_{ps} describes events uniformly distributed over the Dalitz plot; it is a constant and is normalized as described above. We have given the ρ Breit-Wigner distribution elsewhere [1]; it was found that the fraction of Δ is insensitive to the assumed ρ shape so that the details of the ρ analysis do not concern us here.

Table 1
Reaction $\gamma_V p \to p\pi^+\pi^-$: percentages of Δ^{++}, ρ, Δ^0 and phase-space production as obtained from maximum likelihood fits to the Dalitz plot

W (GeV)	Q^2 (GeV^2)	$\pi^-\Delta^{++}$	$p\rho^0$	$\pi^+\Delta^0$	Phase space
	0	91 ± 2 [a]		0 [a]	10 ± 1 [a]
1.3–1.5	0.3 – 0.5	77 ± 8		6 ± 6	17 ± 10
	0.5 – 0.8	66 ± 9		0 ± 1	34 ± 7
	0.8 – 1.4	57 ± 21		8 ± 12	35 ± 6
	0	64 ± 2 [a]	8 ± 2 [a]	16 ± 2 [a]	12 ± 4 [a]
1.5–1.7	0.3 – 0.5	58 ± 5	7 ± 6	10 ± 3	25 ± 11
	0.5 – 0.8	48 ± 5	13 ± 5	18 ± 4	21 ± 9
	0.8 – 1.4	56 ± 7	17 ± 15	22 ± 5	6 ± 17
	0	32 ± 2 [a]	49 ± 5 [b]	3 ± 2 [a]	16 ± 4 [b]
1.7–2.0	0.3 – 0.5	32 ± 3	44 ± 7	1 ± 1	23 ± 6
	0.5 – 0.8	28 ± 3	48 ± 8	6 ± 4	19 ± 6
	0.8 – 1.4	25 ± 3	30 ± 10	4 ± 2	41 ± 6
	0	24 ± 2 [a]	58 ± 5 [a]	1 ± 1 [a]	17 ± 6 [a]
2.0–2.2	0.3 – 0.5	26 ± 5	36 ± 4	8 ± 3	30 ± 4
	0.5 – 0.8	16 ± 4	34 ± 5	5 ± 2	45 ± 4
	0.8 – 1.4	20 ± 8	45 ± 6	1 ± 4	34 ± 5
	0	12 ± 1 [c]	68 ± 4 [c]	2 ± 1 [c]	18 ± 4 [c]
2.2–2.8	0.3 – 0.5	10 ± 2	52 ± 5	3 ± 2	35 ± 4
	0.5 – 0.8	14 ± 5	53 ± 4	2 ± 2	31 ± 7
	0.8 – 1.4	16 ± 6	29 ± 5	1 ± 2	54 ± 8

[a] Results obtained from table 4 of ref. [6b] by averaging over the appropriate W interval.
[b] These values were determined by refitting the data of ref. [16] with a variable ρ shape.
[c] Results from ref. [8].

In a first set of fits the Δ mass and width were determined. At all energies we obtained $\Gamma_\Delta = 110$ MeV. For $W < 1.7$ GeV, $m_\Delta = 1232$ MeV; for higher energies the fit required $m_\Delta = 1220$ MeV. In the subsequent fits m_Δ and Γ_Δ were kept at the above values. The fitted fractions of Δ^{++}, Δ^0, ρ^0 and the phase-space contribution are listed in table 1; for comparison photoproduction results are also given. The relative contribution of Δ^{++} to the channel $\gamma_V p \to p\pi^+\pi^-$ is found to be essentially independent of Q^2; the amount of Δ^0 production is smaller by a factor 5–10 than Δ^{++} production.

4. The reaction $\gamma_V p \to \pi^- \Delta^{++}$

4.1. The Δ^{++} cross section

We show in fig. 1 and table 2 the Δ^{++} cross section as a function of W for $0.3 < Q^2 < 1.4$ GeV^2 and for $Q^2 = 0$ [16]. The W dependence of Δ^{++} production at $\langle Q^2 \rangle = 0.7$ GeV^2 is evidently similar to that for $Q^2 = 0$; namely it exhibits a sharp rise above threshold to a peak between 1.4 and 1.7 GeV followed by a steady fall with increasing energy. In fig. 2 and table 3 we give the cross section in different W intervals as a function of Q^2. To guide the eye, we draw curves of a VDM type, $\sigma(Q^2) = \sigma(0)/(1 + Q^2/m_\rho^2)^2$. With the exception of the W interval 1.7 to 2.0 GeV the curves fit the data points well and demonstrate the approximate W independence of the shape of the Q^2 distributions.

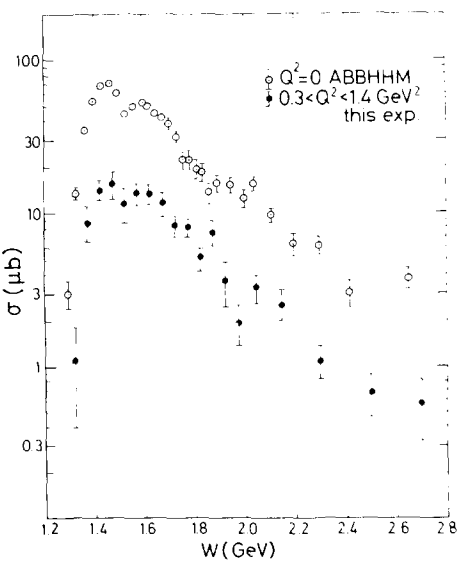

Fig. 1. $\sigma(\gamma_V p \to \pi^- \Delta^{++})$ as a function of W for $0.3 < Q^2 < 1.4$ GeV^2(•). The open points are ABBHHM data [16] from table 4 of ref. [6b].

Table 2
Cross sections for $\gamma_V p \to \pi^- \Delta^{++}$ as a function of W for $0.3 < Q^2 < 1.4$ GeV^2

W (GeV)	$\sigma_T + \epsilon\sigma_L$ (μb)
1.25 – 1.30	0.2 ± 0.2
1.30 – 1.35	1.1 ± 0.7
1.35 – 1.40	8.7 ± 2.3
1.40 – 1.45	14.2 ± 2.1
1.45 – 1.50	15.4 ± 2.9
1.50 – 1.55	11.5 ± 2.8
1.55 – 1.60	13.5 ± 2.2
1.60 – 1.65	13.4 ± 1.8
1.65 – 1.70	11.6 ± 2.1
1.70 – 1.75	8.3 ± 1.3
1.75 – 1.80	8.1 ± 1.0
1.80 – 1.85	5.1 ± 0.8
1.85 – 1.90	7.5 ± 1.4
1.90 – 1.95	3.6 ± 1.2
1.95 – 2.00	2.0 ± 0.6
2.00 – 2.10	3.3 ± 0.7
2.10 – 2.20	2.5 ± 0.6
2.20 – 2.40	1.1 ± 0.3
2.40 – 2.60	0.7 ± 0.2
2.60 – 2.80	0.6 ± 0.2

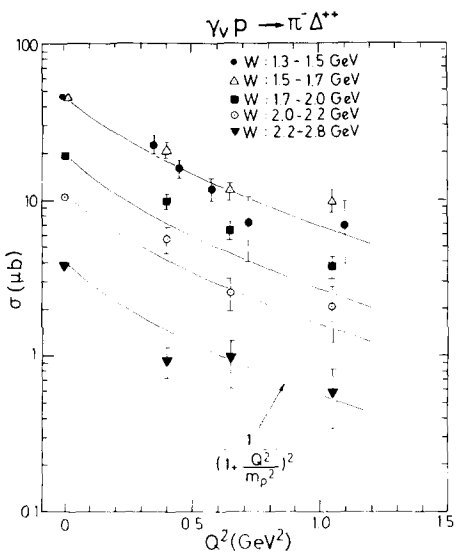

Fig. 2. $\sigma(\gamma_V p \to \pi^- \Delta^{++})$ as a function of Q^2 for different W regions. The $Q^2 = 0$ points were interpolated from table 4 of ref. [6b].

Table 3
Cross sections for $\gamma_V p \to \pi^- \Delta^{++}$ as a function of Q^2 for different W intervals

W (GeV)	Q^2 (GeV^2)	$\sigma_T + \epsilon\sigma_L$ [a] (μb)
1.30 – 1.50	0.3 – 0.4	23.0 ± 3.1
	0.4 – 0.5	16.1 ± 1.9
	0.5 – 0.65	11.7 ± 1.8
	0.65 – 0.80	7.2 ± 3.2
	0.80 – 1.40	6.9 ± 3.0
1.50 – 1.70	0.30 – 0.50	20.8 ± 2.0
	0.50 – 0.80	11.3 ± 1.4
	0.80 – 1.30	9.8 ± 1.6
1.70 – 2.0	0.30 – 0.50	9.9 ± 1.0
	0.50 – 0.80	6.4 ± 0.8
	0.80 – 1.30	3.7 ± 0.6
2.0 – 2.20	0.30 – 0.50	5.6 ± 1.1
	0.50 – 0.80	2.5 ± 0.6
	0.80 – 1.30	2.0 ± 0.8
2.20 – 2.80	0.30 – 0.50	0.9 ± 0.2
	0.50 – 0.80	1.0 ± 0.4
	0.80 – 1.30	0.6 ± 0.2

[a] The cross sections given in table 3 and fig. 2 have been renormalized by 5–20% to match the averaged cross sections of table 2 and fig. 1; i.e., we enforced

$$\left.\frac{\Sigma \Delta W \sigma(W)}{\Sigma \Delta W}\right|_{\text{table 2}} = \left.\frac{\Sigma \Delta Q^2 \sigma(Q^2)}{\Sigma \Delta Q^2}\right|_{\text{table 3}} .$$

The summation was performed in each of the five W intervals of table 3. This renormalisation has not been applied in ref. [10].

4.2. Δ^{++} production angular distribution

The differential cross sections $d\sigma/d\Omega$ and $d\sigma/dt$ were determined by separate Dalitz-plot fits for each interval of $\cos\theta_{CMS}$ and t (here θ_{CMS} is the Δ^{++} production angle with respect to the proton direction in the $\gamma_V p$ c.m.s. and t is the four-momentum transfer squared from proton to Δ). The results for $d\sigma/d\Omega$ are given in fig. 3 for different W intervals. In all W intervals shown the production angular distribution is anisotropic with a forward peak; the anisotropy increases with increasing W. Also shown in fig. 3 are the photoproduction differential cross sections [16] (open points) scaled down by a factor four. In general, the shapes of the photo- and electroproduction angular distributions agree, which indicates that the Δ^{++} production mechanisms are similar at $Q^2 = 0$ and in the region $0.3 < Q^2 < 1.4$ GeV^2. Fig. 4 and

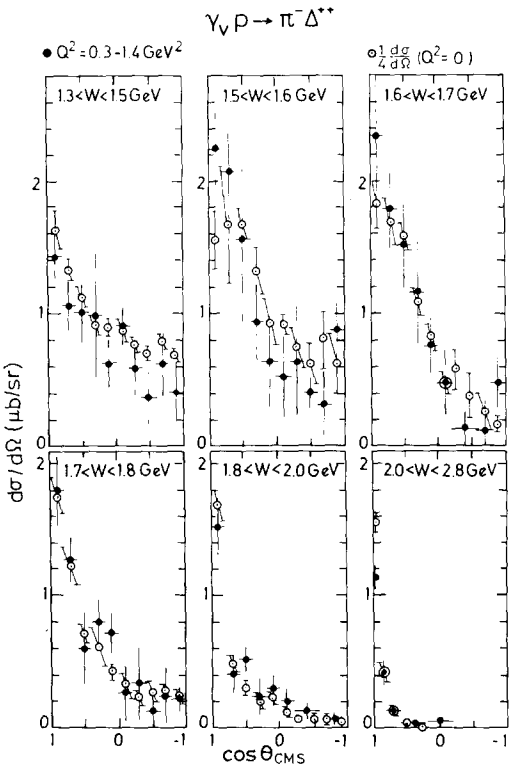

Fig. 3. Differential cross sections $d\sigma/d\Omega$ for $\gamma_v p \to \pi^- \Delta^{++}$ for different W regions. The open points are photoproduction cross sections scaled down by a factor 4. We obtained the $Q^2 = 0$ cross sections by refitting the data of ref. [16] in appropriate W intervals using the fitting procedure of subsect. 3.2.

table 4 give $d\sigma/dt$ for photo- and electroproduction for the region $1.7 < W < 2.0$ GeV* and $2.0 < W < 2.8$ GeV. The figure shows that the slope of the forward peak is lower in electroproduction than in photoproduction. At large $|t|$, the electroproduction and photoproduction cross sections are equal within errors, in agreement with a previous measurement [17].

4.3. The Δ^{++} decay angular distribution

In order to determine the spin dependence of the Δ^{++} production mechanism, we have studied the decay angular distribution of the Δ^{++} using the formalism given in detail in the appendix.

* The difference between the photoproduction and the electroproduction $d\sigma/d\Omega$ and $d\sigma/dt$ plots for $1.7 < W < 2.0$ GeV may be understood in terms of the change of t_{min} and t_{max} with W and Q^2.

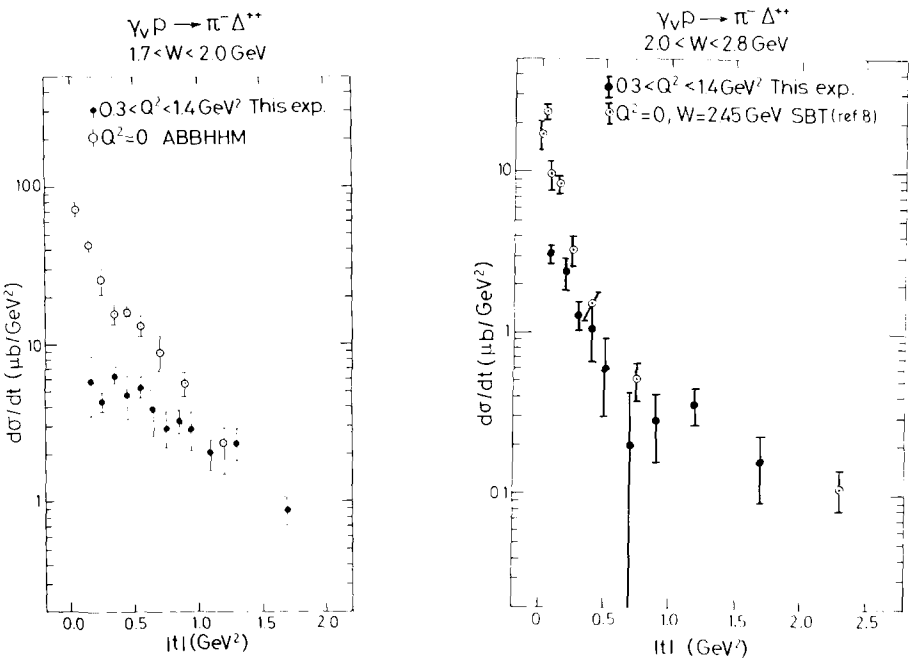

Fig. 4. $d\sigma/dt$ for $\gamma_V p \to \pi^- \Delta^{++}$. (a) $1.7 < W < 2.0$ GeV, (b) $2.0 < W < 2.8$ GeV. The open points are photoproduction data from refs. [8,16]. We obtained the $Q^2 = 0$ cross section in fig. 4a by refitting the data of ref. [16] in the appropriate W interval.

The Δ^{++} decay was studied in the Gottfried-Jackson system which is also used in the analysis of Δ^{++} photoproduction [6,8,16]. The incoming proton direction in the Δ rest frame is taken as the z direction, the normal to the production plane as the y direction. The Δ^{++} decay is described by the polar and azimuthal angles θ and ϕ of the decay proton with respect to these axes. We also use the angle Φ of the polarization vector of the transverse photons in the hadron c.m.s., which is the angle between the Δ^{++} production plane and the electron scattering plane.

We analysed the Δ^{++} decay distribution $W(\cos\theta, \phi, \Phi)$ in terms of the Δ density matrix in the Gottfried-Jackson system [9,20]. The density matrix elements were determined by the method of moments weighting each event with the maximum-likelihood weight factor $W^i_\Delta \propto a_\Delta F_\Delta(m^i_{p\pi^+})$; for details of the method see refs. [10, 18]. We estimate that the effects of background lead to systematic uncertainties that are less than the statistical errors. The density matrix elements, r^{04}, are given in fig. 5 as a function of the production angle for different W intervals with $0.3 < Q^2 < 1.4$ GeV^2. In fig. 6, the r^{04} elements are given as a function of production angle for different W and Q^2 intervals. The remaining density matrix elements are small and are given in ref. [10]. The traces of the matrices r^1 and r^5 are given in table 5 as a function of W.

Table 4
Reaction $\gamma_V p \to \pi^- \Delta^{++}$: differential cross sections for $0.3 < Q^2 < 1.4$ GeV^2

$1.7 < W < 2.0$ GeV				$2.0 < W < 2.8$ GeV			
$\lvert t\rvert$ (GeV^2)	$d\sigma/dt$ (μb/GeV^2)	$\langle \Delta t \rangle$ (GeV^2)	$\langle Q^2 \rangle$ (GeV^2)	$\lvert t\rvert$ (GeV^2)	$d\sigma/dt$ (μb/GeV^2)	$\langle \Delta t \rangle$ (GeV^2)	$\langle Q^2 \rangle$ (GeV^2)
0.1 – 0.2	5.9 ± 2.4	0.078	0.425	0.05 – 0.15	3.2 ± 0.4	0.070	0.480
0.2 – 0.3	4.3 ± 0.6	0.095	0.463	0.15 – 0.25	2.4 ± 0.6	0.098	0.491
0.3 – 0.4	6.4 ± 0.7	0.098	0.463	0.25 – 0.35	1.3 ± 0.3	0.1	0.526
0.4 – 0.5	4.8 ± 1.5	0.1	0.511	0.35 – 0.45	1.1 ± 0.4	0.1	0.529
0.5 – 0.6	5.4 ± 0.8	0.1	0.523	0.45 – 0.60	0.6 ± 0.3	0.15	0.506
0.6 – 0.7	3.9 ± 1.2	0.1	0.518	0.60 – 0.80	0.2 ± 0.2	0.2	0.538
0.7 – 0.8	2.9 ± 0.7	0.1	0.552	0.80 – 1.00	0.3 ± 0.1	0.2	0.530
0.8 – 0.9	3.3 ± 0.6	0.1	0.525	1.00 – 1.40	0.4 ± 0.1	0.4	0.566
0.9 – 1.0	2.9 ± 0.8	0.1	0.539	1.40 – 2.00	0.2 ± 0.1	0.60	0.585
1.0 – 1.2	2.0 ± 0.4	0.2	0.574	2.00 –	0.04 ± 0.04	1.472	0.597
1.2 – 1.4	2.3 ± 0.5	0.198	0.572				
1.4 – 2.0	0.9 ± 0.2	0.501	0.662				
2.0 –	0.1 ± 0.3	0.455	0.781				

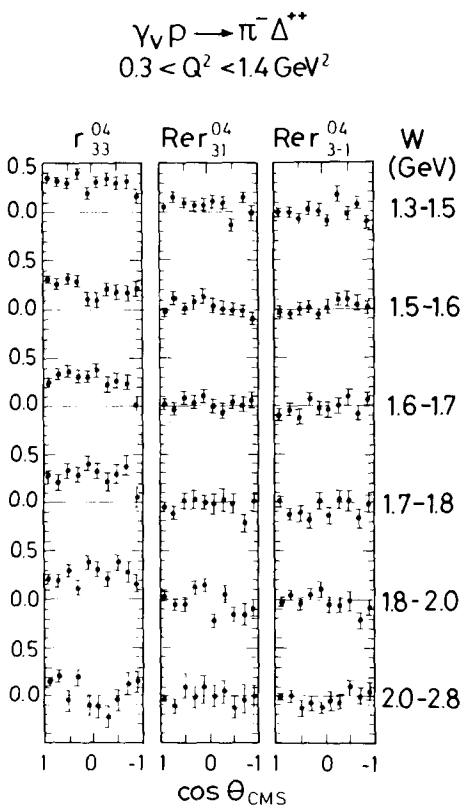

Fig. 5. Δ^{++} density matrix elements in the Gottfried-Jackson system as a function of $\cos\theta_{CMS}$ for different W regions and $0.3 < Q^2 < 1.4$ GeV^2.

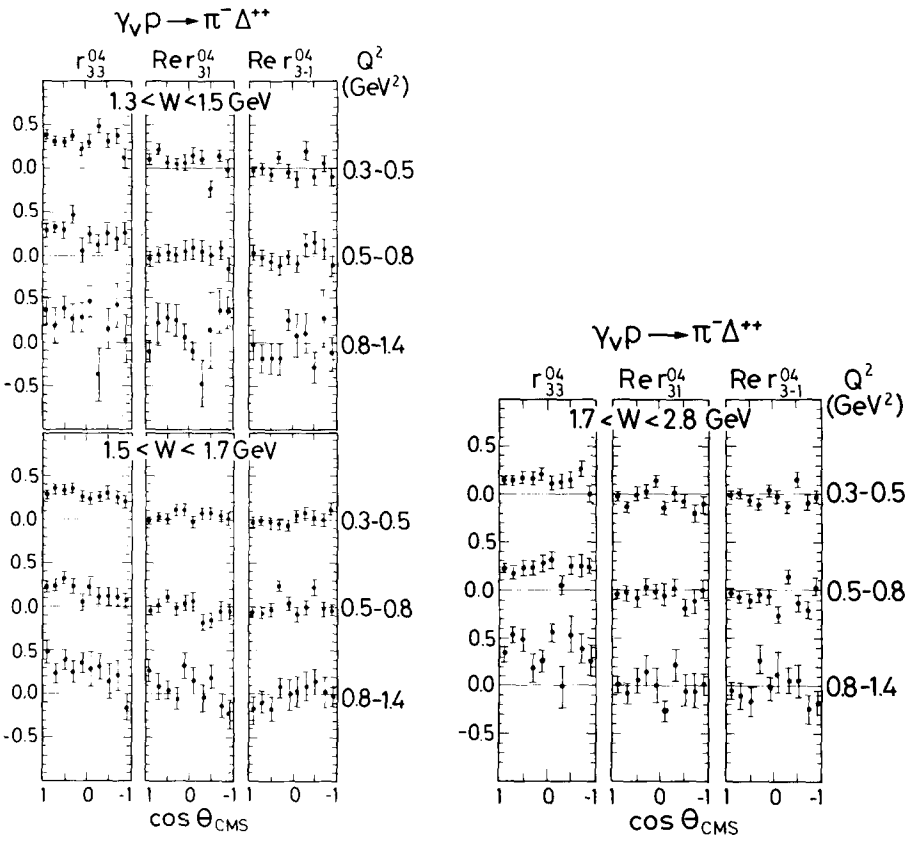

Fig. 6. Δ^{++} density matrix elements in the Gottfried-Jackson system as a function of $\cos\theta_{CMS}$ for different Q^2 and W regions.

In summary we find:

(a) At threshold ($1.3 < W < 1.5$ GeV) $r_{33}^{04} = 0.31 \pm 0.02$; it is independent of production angle and Q^2. For comparison, a pure contact term would give $r_{33}^{04} = 0.375$ * while pure pion exchange would give $r_{33}^{04} = 0$. Absorption corrections to one-pion exchange would increase the expected value of r_{33}^{04}.

(b) With increasing energy r_{33}^{04} decreases. For $W > 1.7$ GeV, r_{33}^{04} becomes Q^2 dependent, increasing as Q^2 increases, and is dependent upon the production angle (fig. 5). This indicates the increasing importance of one-pion exchange at small Q^2 ($0.3 < Q^2 < 0.8$ GeV^2).

(c) The trace of r^1, i.e., $2(r_{11}^1 + r_{33}^1)$, is energy dependent, being ~0 at threshold

* Strictly speaking this holds only in the forward direction where the longitudinal contribution vanishes.

Table 5
Reaction $\gamma_v p \to \pi^- \Delta^{++}$: trace of density matrices r^1 and r^5 in the Gottfried-Jackson system for $0.3 < Q^2 < 1.4$ GeV^2

W(GeV)	Tr r^1	Tr r^5
1.30 – 1.50	0.0 ± 0.05	0.01 ± 0.02
1.50 – 1.60	0.0 ± 0.05	−0.03 ± 0.02
1.60 – 1.70	−0.04 ± 0.05	−0.09 ± 0.03
1.70 – 1.80	−0.04 ± 0.06	−0.06 ± 0.03
1.80 – 2.00	−0.15 ± 0.06	−0.04 ± 0.03
2.00 – 2.80	−0.17 ± 0.07	−0.10 ± 0.03

and becoming negative at higher W (see table 5). Since for transverse photons,

$$P_\sigma^t = \frac{\sigma_n^t - \sigma_u^t}{\sigma_n^t + \sigma_u^t} = 2(\rho_{11}^1 + \rho_{33}^1) = 2(1 + \epsilon R)(r_{11}^1 + r_{33}^1) ,$$

where $\sigma_n(\sigma_u)$ are the cross sections for Δ production through natural (unnatural) parity exchange in the t-channel, the values of tr r^1 imply $\sigma_n \sim \sigma_u$ at threshold and $\sigma_u > \sigma_n$ for $W > 1.8$ GeV. This is consistent with dominance of a contact term at threshold and of one pion exchange at higher energies.

(d) The value of tr r^5 measures the longitudinal-transverse interference cross section σ_I, through the relation

$$\text{tr } r^5 = -\frac{2\sigma_I}{\sigma_T + \epsilon\sigma_L} .$$

At small W, tr r^5 is compatible with zero; for $W > 2.0$ GeV, tr $r^5 = -0.10 \pm 0.03$, in agreement with other measurements [19].

In general, the density matrix elements discussed above agree with those found in photoproduction [6,16]. Thus the Δ^{++} decay angular distributions, like the production angular distributions, indicate that the same mechanisms are important in electro- and photoproduction.

5. The reaction $\gamma_v p \to \pi^+ \Delta^0$

It has been found in photoproduction that strong Δ^{++}-Δ^0 interference occurs at low W [6]. Consequently the maximum-likelihood fit to the Dalitz plot density (eq. (8)) was modified by the addition of an interference term between the Δ production amplitudes (for full details see ref. [10]). This introduces two new parameters: α, the degree of coherence between the Δ^{++} and Δ^0 amplitudes, and ϕ, the phase difference between the amplitudes. In all fits the statistical significance of the interference is weak and therefore we present our results both with and without interference; for $W > 1.8$ GeV the overlap between the Δ bands is small, so the interference can be neglected. At all energies the effect of the Δ^0 on the Δ^{++} quantities (such as the cross section and density matrix elements) is negligible.

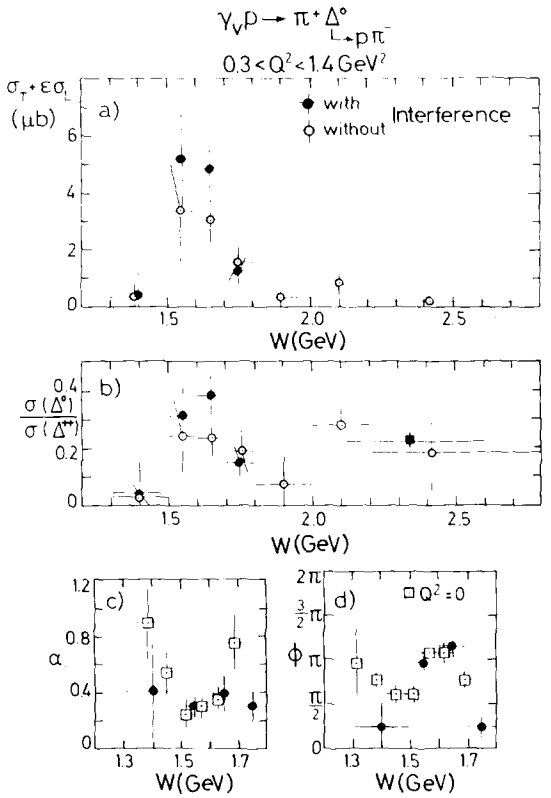

Fig. 7. Reaction $\gamma_v p \to \pi^+ \Delta^0$ ($\Delta^0 \to \pi^- p$) for $0.3 < Q^2 < 1.4\ GeV^2$. (a) $\sigma(\gamma_v p \to \pi^+ \Delta^0)$ as a function of W, (b) $\sigma_v p \to \pi^+ \Delta^0)/\sigma(\gamma_v p \to \pi^- \Delta^{++})$ as a function of W. The full and the open points in fig. 7a, b were obtained from fits with and without interference, respectively. (c), (d) the $\Delta^{++} - \Delta^0$ interference parameters, α, ϕ as a function of W. Also shown are the photoproduction values from ref. [6] (open squares).

In fig. 7a we show the cross section for $\gamma_v p \to \pi^+ \Delta^0 (\Delta^0 \to p\pi^-)$ as a function of W. We find a maximum between 1.5 and 1.7 GeV followed by a strong fall-off at higher energies. The ratio, R_Δ, of the Δ^0 and Δ^{++} cross sections is given in fig. 7b. Figs. 7c and 7d give the fit parameters α and ϕ together with those from photoproduction [6] (open points). Within errors, our results agree with those from photoproduction.

Fig. 8 shows the Q^2 dependence of the Δ^0 cross section and of R_Δ in different W intervals. With the exception of the region $1.5 < W < 1.7$ GeV where there is a trend for Δ^0 production to be less Q^2 dependent than Δ^{++} production, Δ^0 and Δ^{++} production have similar Q^2 dependences. The full squares in figs. 7b, 8 are data points from ref. [19] at $t - t_{min} = 0.04\ GeV^2$. They are consistent with our data.

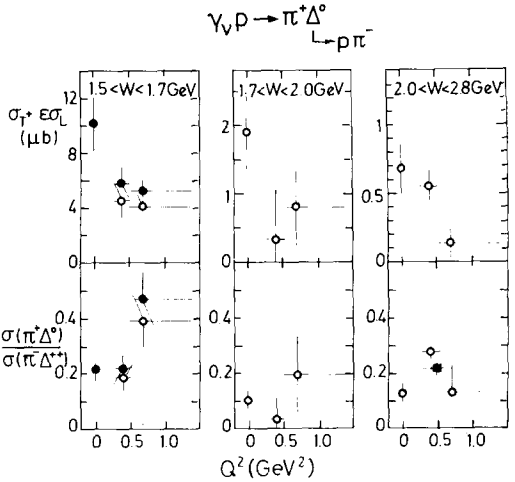

Fig. 8. Cross section $\sigma(\gamma_v p \to \pi^+ \Delta^0)$ and cross section ratio $\sigma(\pi^+\Delta^0)/\sigma(\pi^-\Delta^{++})$ as a function of Q^2 for three W regions. The points at Q^2 are from ref. [6]. The meaning of the full and open points is the same as in fig. 7a and b. Also shown is a measurement from ref. [19] (■).

6. Summary

We have studied the reactions $\gamma_v p \to \pi^- \Delta^{++}$ and $\gamma_v p \to \pi^+ \Delta^0$ in the kinematic region $0.3 < Q^2 < 1.4$ GeV^2, $W < 2.8$ GeV. We find that:

(a) The cross section for Δ^{++} production shows a W dependence which is similar to that found in photoproduction (fig. 1).

(b) The dominating forward Δ^{++} cross section depends on Q^2 approximately as $1/(1 + Q^2/m_\rho^2)^2$, i.e., it shows a stronger Q^2 dependence than the total inelastic $\gamma_v p$ cross section. This Q^2 behaviour is also observed in the total Δ^{++} production cross section in nearly all W intervals (fig. 2). In contrast Δ^{++} production at large $|t|$ shows a weak Q^2 dependence for $W > 2$ GeV.

(c) At all energies the Δ^{++} production angular distribution is anisotropic with a forward peak (with respect to the incoming proton in the hadron c.m.s.) which narrows as W increases. The shape of the production angular distribution is similar to that found in photoproduction (fig. 3).

(d) For $W > 1.8$ GeV unnatural parity exchange dominates over natural parity exchange in the t-channel as expected for one-pion exchange.

(e) For Δ^0 production, the W dependence of the cross section, the ratio to Δ^{++} production, and the phase angle between the Δ^0 and Δ^{++} production amplitudes, are similar to the corresponding quantities found in photoproduction.

In conclusion, our observations for small momentum transfer, $|t|$, are compatible with Δ electroproduction occurring through the same mechanisms as in photoproduction with the Q^2 dependence of the cross section being determined by a VDM-

like ρ propagator. At large momentum transfers Δ^{++} production shows a weak Q^2 dependence.

We thank C. Benz, I. Bloodworth, D. Hoffmann, W. Kraus, B. Naroska, D. Notz, W.J. Podolsky, C. Sander, K. Smith, P. Stein, and S. Yellin for their help in the early stages of this experiment. We thank also N. Gollmer, E. Hell, V. Heynen, A. Huber, H. Klinkmüller, G. Kraft, H.H. Sabath, S.W. Sass, K. Westphal, and K.H. Wroblewski for their technical assistance. We acknowledge the excellent performance of the Synchrotron crew, the Hallendienst and the Kältetechnik. The cooperation by Mr. Kuhlmann and the Rechenzentrum has been invaluable. We thank our scanning and measuring staffs for their careful work. The Glasgow members of the collaboration thank the DESY Directorate for their kind hospitality. The work at Hamburg has been supported by the Bundesministerium für Forschung und Technologie, the work at Glasgow by the Science Research Council.

Appendix

Decay angular distributions and density matrix formalism for Δ decay

The Δ decay is analyzed in the Gottfried-Jackson system. The z axis of this system is taken as the direction of the incoming proton, p, in the Δ rest frame, the y axis as the normal to the production plane. As the analyser of the Δ decay we use the decay proton p′; thus the decay of the Δ is defined by the polar and azimuthal angles θ, ϕ given by

$$\cos\theta = \frac{p \cdot p'}{|p||p'|},$$

$$\cos\phi = \frac{(\gamma_v \times \pi^-) \cdot (p \times p')}{|\gamma_v \times \pi^-||p \times p'|},$$

$$\sin\phi = -\frac{((\gamma_v \times \pi^-) \times p) \cdot (p \times p')}{|(\gamma_v \times \pi^-) \times p||p \times p'|},$$

where the symbols represent the 3 vectors of the corresponding particles in the Δ rest frame.

The decay distribution can also depend on the angle Φ of the polarization vector of the transverse photons in the hadron c.m.s.; Φ is given by the angle between the Δ production plane and the electron scattering plane

$$\cos\Phi = \frac{(\gamma_v \times \pi^-) \cdot (e \times e')}{|\gamma_v \times \pi^-||e \times e'|},$$

$$\sin\Phi = \frac{((\gamma_v \times \pi^-) \times (e \times e')) \cdot \gamma_v}{|\gamma_v \times \pi^-||e \times e'||\gamma_v|},$$

where the symbols represent the 3 vectors of the corresponding particles in the hadron c.m.s.; e, e′ are the incident and scattered electron.

The Δ decay angular distribution, $W(\cos\theta, \phi, \Phi)$, can be expressed in terms of the Δ density matrix using the formalism of ref. [20] by:

$$W(\cos\theta, \phi, \Phi) = \frac{1}{1+\epsilon R}\,[W^0(\cos\theta, \phi) - \epsilon\cos 2\Phi\, W^1(\cos\theta, \phi) - \epsilon\sin 2\Phi\, W^2(\cos\theta, \phi) + \epsilon R W^4(\cos\theta, \phi) + \sqrt{2\epsilon(\epsilon+1)}\sqrt{R}\,\{\cos\Phi\, W^5(\cos\theta, \phi) + \sin\Phi\, W^6(\cos\theta, \phi)\}],$$

where

$$R = \frac{\sigma_L(\gamma_v p \to \Delta^{++}\pi^-)}{\sigma_T(\gamma_v p \to \Delta^{++}\pi^-)},$$

and

$$W^\alpha(\cos\theta, \phi) = \frac{3}{4\pi}\{\rho^\alpha_{33}\sin^2\theta + (\tfrac{1}{2} - \rho^\alpha_{33})(\tfrac{1}{3} + \cos^2\theta) - \frac{2}{\sqrt{3}}\mathrm{Re}\,\rho^\alpha_{31}\cos\phi\sin 2\theta - \frac{2}{\sqrt{3}}\mathrm{Re}\,\rho^\alpha_{3-1}\cos 2\phi\sin^2\theta\}$$

for $\alpha = 0$ and 4,

$$W^\alpha(\cos\theta, \phi) = \frac{3}{4\pi}\{\rho^\alpha_{33}\sin^2\theta + \rho^\alpha_{11}(\tfrac{1}{3} + \cos^2\theta) - \frac{2}{\sqrt{3}}\mathrm{Re}\,\rho^\alpha_{31}\cos\phi\sin 2\theta - \frac{2}{\sqrt{3}}\mathrm{Re}\,\rho^\alpha_{3-1}\cos 2\phi\sin^2\theta\}$$

for $\alpha = 1$ and 5,

$$W^\alpha(\cos\theta, \phi) = \frac{3}{4\pi}\left\{\frac{2}{\sqrt{3}}\mathrm{Im}\,\rho^\alpha_{31}\sin\phi\sin 2\theta + \frac{2}{\sqrt{3}}\mathrm{Im}\,\rho^\alpha_{3-1}\sin 2\phi\sin^2\theta\right\}$$

for $\alpha = 2$ and 6.

Since R is not known, ρ^0 and ρ^4 cannot be separately determined. Thus we determine only the combinations

$$r^{04}_{ik} = \frac{\rho^0_{ik} + R\,\rho^4_{ik}}{1+\epsilon R}.$$

Similarly we can measure only the quantities

$$r^\alpha_{ik} = \frac{\rho^\alpha_{ik}}{1+\epsilon R}, \qquad \text{for } \alpha = 1 \text{ and } 2,$$

$$r^{\alpha}_{ik} = \frac{\sqrt{R}}{1+\epsilon R}\,\rho^{\alpha}_{ik}\,, \qquad \text{for } \alpha = 5 \text{ and } 6\,.$$

From the density matrix elements we can derive two quantities of particular interest in the experiment, namely P^t_σ, which measures the mixture of natural and unnatural parity exchange cross sections, σ_n, σ_u, in the t-channel for transverse photons, and σ_I which measures transverse-longitudinal interference.

P^t_σ is given by [21]

$$P^t_\sigma = \frac{\sigma^t_n - \sigma^t_u}{\sigma^t_n + \sigma^t_u} = 2(\rho^1_{11} + \rho^1_{33}) = 2(1+\epsilon R)(r^1_{11} + r^1_{33})\,,$$

and

$$\sigma_I = -\tfrac{1}{2}\,\mathrm{tr}\, r^5(\sigma_T + \epsilon\sigma_L)\,.$$

References

[1] P. Joos et al., Nucl. Phys. B113 (1976) 53.
[2] P. Joos et al., Nucl. Phys. B122 (1977) 365.
[3] C.K. Chen et al., Nucl. Phys. B133 (1978) 13;
J.M. Scarr et al., Nucl. Phys. B135 (1978) 224.
[4] P. Joos et al., Phys. Lett. 52B (1974) 481.
[5] P. Joos et al., Phys. Lett. 62B (1976) 230.
[6a] D. Lüke and P. Söding, Springer Tracts in Modern Physics 59 (1971) 39;
[6b] D. Lüke, Thesis, Internal report DESY F1-72/7 (1972), unpublished.
[7] A.M. Boyarski et al., Phys. Rev. Lett. 22 (1969) 148.
[8] J. Ballam et al., Phys. Rev. D5 (1972) 545.
[9] V. Eckardt et al., Nucl. Phys. B55 (1973) 45;
E. Rabe, Thesis, Internal report DESY F1-74/2 (1974), unpublished.
[10] K. Wacker, Thesis, Internal report DESY F1-76/04 (1976), unpublished.
[11] C. Sander, Diploma thesis, Internal report DESY F1-75/3 (1975), unpublished.
[12] L.Y. Mo and Y.S. Tsai, Rev. Mod. Phys. 41 (1969) 205.
[13] S. Stein et al., Phys. Rev. D12 (1975) 1884.
[14] L. Hand, Phys. Rev. 129 (1963) 1834.
[15] G. Wolf, Phys. Rev. 182 (1969) 1538.
[16] ABBHHM Collaboration, Phys. Rev. 175 (1968) 1669.
[17] H.E. Montgomery et al., Nucl. Phys. B51 (1973) 377.
[18] P.E. Condon and P.L. Cowell, Phys. Rev. D9 (1974) 2558.
[19] I. Dammann et al., Nucl. Phys. B54 (1973) 355.
[20] K. Schilling and G. Wolf, Nucl. Phys. B61 (1973) 381;
G. Wolf, unpublished.
[21] P. Stichel, Z. Phys. 180 (1964) 170.